

Strangeness and Quark Gluon Plasma

Johann Rafelski[†] and Jean Letessier^{‡†}

[†] Department of Physics, University of Arizona, Tucson, AZ 85721

[‡] Laboratoire de Physique Théorique et Hautes Energies
Université Paris 7, 2 place Jussieu, F-75251 Cedex 05.

Abstract. A brief summary of strangeness mile stones is followed by a chemical non-equilibrium statistical hadronization analysis of strangeness results at SPS and RHIC. Strange particle production in AA interactions at $\sqrt{s_{NN}} \geq 8.6$ GeV can be understood consistently as originating from the deconfined quark-gluon plasma in a sudden hadronization process. Onset of QGP formation as function of energy is placed in the beam energy interval 10–30A GeV/c. Strangeness anomalies at LHC are described.

PACS numbers: 12.38.Mh

Submitted to: *J. Phys. G: Nucl. Phys.*

1. Introduction

We consider, in a chemical analysis of yields, the strange hadron production in A–A collisions at the SPS and RHIC. We find that these results can be well understood and consistently described within the Fermi type, chemical near-equilibrium, statistical hadronization model [1, 2, 3]. We find that the deviation from equilibrium conditions are most pronounced at RHIC ($\sqrt{s_{NN}} = 130$ GeV, RHIC₁₃₀) [4, 5], with the conditions of hadronization strongly deviating from chemical equilibrium. The present analysis and reanalysis of the results obtained in the energy range $19.4 \leq \sqrt{s_{NN}} \leq 8.75$ GeV by NA49 [6, 7, 8, 9, 10, 11, 12] and WA97/NA57 [13, 14, 15, 16] experiments is confirming these features characteristic of the formation of a new state of matter at SPS.

The strongest difference between SPS and RHIC collision results is the order of magnitude enhancement in strange particle yield per participant, this result is not new but has found so far little attention [4, 5]. The strangeness yield rise increases compared to SPS [2, 3] in a manner which is more spectacular than the increase in the total hadron multiplicity. This is an expression of the increase of the excess of strangeness (greater chemical nonequilibrium) at RHIC as compared to SPS. We establish this increase in strangeness yield with precision, which requires use of an appropriate analysis tool of hadron multiplicities, which allows reliable and precise description of the unobserved particle phase space in domains not yet experimentally accessible.

At RHIC₁₃₀, each baryon participant leads to formation of nearly 9 strange quark pairs in Au–Au reactions. We show in section 5 that this high yield is reached gradually as function of the available fireball thermal energy. This is confirming that this high

yield of strangeness is result of the same physical process in all reaction energies considered here, beginning with $\sqrt{s_{NN}} = 8.75$ GeV (corresponding to a $40A$ GeV beam on laboratory stationary target). We also present in section 5 how the diverse properties of the hadronic fireball change as function of energy. The introduction of chemical nonequilibrium leads to a rather low hadronization temperature which we interpret in section 6. where we discuss in depth at which energy domain the onset of QGP may be occurring.

Before we turn to this part of our report a brief introduction to ‘strangeness’ the important mile stones of 10 years of experimental research are presented in the following section 2. This is followed in section 3 by a discussion of the mechanism of QCD based production of strangeness in a quark–gluon plasma (QGP). In particular we show that the gluon fusion processes in QGP is capable to populate within the reaction time the strange quark phase space [17, 18, 19, 20], up to, and even above the chemical equilibrium yield in the QGP phase [20].

The other QCD based process, light quark–antiquark fusion into strange quark pair, has been earlier shown to be too slow for strangeness equilibration in the QGP [21, 22]. Thus the discovery of the dominance of the gluon fusion process has been the key stepping stone in establishing strangeness as an observable of QGP. The computation presented in section 3 is assuming early thermalization, and following rapid collective evolution. This scenario is today viewed as a very likely reaction sequence, seen the behavior of the v_2 flow parameter, especially so that it applies also to strange hadrons [23].

A very important aspect of the study of strange particles produced by QGP is the final state hadron production process. We present the essential elements of statistical hadronization in section 4. These principles are employed in section 5, in analysis of the RHIC and SPS results, and as noted a synthesis of our analysis and their impact for the search of the onset of QGP formation is offered in section 6. In the final section 7 we argue that there is a very interesting future for strangeness in the LHC energy domain.

2. Strangeness — a popular QGP diagnostic tool

There are several different strange particles in nature allowing us to study several complementary physics questions. Denoting here light flavors with $q = u, d$ we consider the stable particles:

$$\phi(s\bar{s}), \text{ K}(q\bar{s}), \text{ }\overline{\text{K}}(\bar{q}s), \text{ }\Lambda(qqs), \text{ }\overline{\Lambda}(\bar{q}\bar{q}\bar{s}), \text{ }\Xi(qss), \text{ }\overline{\Xi}(\bar{q}\bar{s}\bar{s}), \text{ }\Omega(sss), \text{ }\overline{\Omega}(\bar{s}\bar{s}\bar{s}).$$

Moreover, the study of strange hadron resonances such as K^* , Σ^* , Λ^* is a very promising avenue of forthcoming research, leading to direct determination of hadronization conditions.

Many strange hadrons are subject to a self analyzing decay within several centimeters from the point of production, as is illustrated in figure 1 for the cascading Ξ^- -decay. Thus one tracking device, typically today a TPC combined with silicon vertex detector allows the measurement of the many particle yields of interest. The accessibility of strange hadron distributions has lead, in recent years, to an explosion of both experimental and theoretical interest. Moreover, production rates of hadronic particles and hence statistical significance even for low intensity beam is usually high.

Multistrange hadrons can be formed in hadronization of QGP by ‘cross talk’ between quarks made in disjoint microscopic reactions [24]. An illustration of this

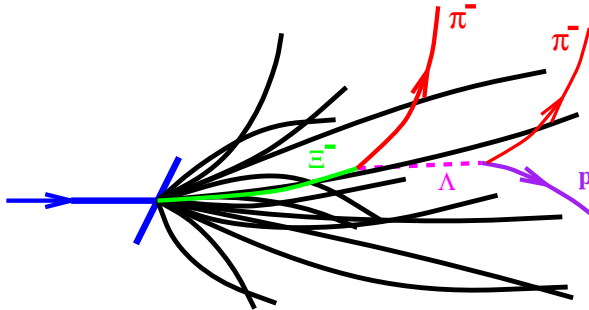


Figure 1. Illustration of the Ξ^- -production by an incoming, e.g., SPS Pb-beam, on a heavy laboratory target, and its subsequent decay. Dashed line depicts the invisible neutral Λ , emerging from the decay kink $\Xi^- \rightarrow \pi^- \Lambda$, and ending in the decay ‘V’ of $\Lambda \rightarrow p + \pi^-$.

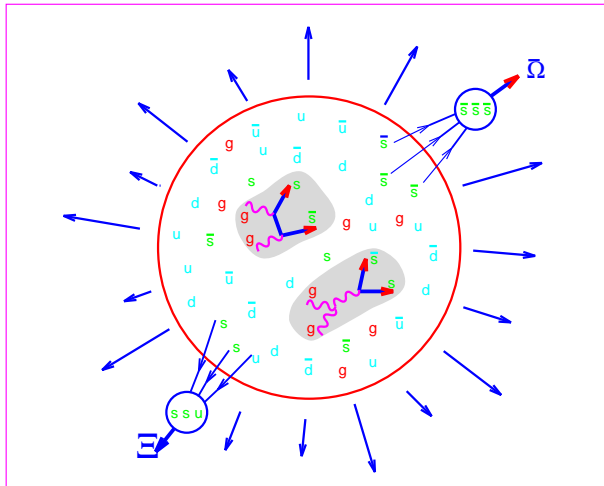


Figure 2. Illustration of the cross-talk two step mechanism of strange hadron formation from QGP: inserts show gluon fusion into strangeness, followed by QGP recombinant hadronization.

process is presented in figure 2: the inserts show gluon fusion processes $gg \rightarrow s\bar{s}$ [17], which establish ample supply of strange quark pairs in the early stages of QGP evolution. In the ensuing hadronization process, quark recombination leads to emergence of particles such as here shown $\Xi(sqq)$, $\bar{\Omega}(\bar{s}\bar{s}\bar{s})$, which otherwise could only very rarely be produced, considering that several rarely occurring processes would have to coincide. Enhancement of such particles is for this reason indicative of deconfinement [17, 25]. This mechanism leads to the expectation that the enhancement of strange antibaryons is progressing with strangeness content, as was recognized and discussed qualitatively already 20 years ago, see e.g., section 4 in [26].

Since the production of strangeness occurs predominantly in thermal gluon fusion $gg \rightarrow s\bar{s}$, see section 3, the overabundant presence of strangeness in high energy relativistic reactions can be on theoretical grounds linked to presence of thermal gluons, and thus to QGP. Beyond the dominant processes $gg \rightarrow s\bar{s}$ there is also, at 10–15% of the total rate, a contribution from $q\bar{q} \rightarrow s\bar{s}$. This rate alone would

however not suffice to equilibrate strangeness in rapidly disintegrating QGP phase formed in relativistic heavy ion collisions [21, 22].

The remarkable coincidence of scales involving the strange quark mass m_s , and the critical temperature of hadronic phase transition T_c ,

$$m_s \simeq T_c \quad \text{which implies} \quad \tau_s \simeq \tau_{\text{QGP}}, \quad (1)$$

allows the $gg \rightarrow s\bar{s}$ production process to act as a clock for the collision reaction. Another interesting feature is that, in a baryon rich environment, we also have $\bar{s} > \bar{q}$ [24], which applies when the quark chemical potential is greater than the mass of the strange quark. In this condition a strange antibaryon enhancement is expected, comparing to the nonstrange antibaryons, including the anomaly $\bar{\Lambda}/\bar{p} > 1$. This should be the case at the lower energy limit of SPS.

In this line of thought, even though there is a near u, d, s flavor symmetry at RHIC, we also expect (anti)hyperon dominance of (anti)baryons in this condition. Here, the mechanism is slightly different [20]: each baryon or antibaryon contains three quarks or, respectively, antiquarks, and it is hard to find in the flavor symmetric pool of quarks (and antiquarks) three non-strange quarks (or antiquarks), in fact the statistical probability for assembly of three nonstrange quarks is 1/3. Thus 2/3 of all produced baryons, or respectively antibaryons, will in limit of flavor symmetry carry strangeness, and this feature of course remains true in the future LHC environment.

Multistrange anti-hyperon abundance ratios were studied extensively and we show in figure 3 the three ratios:

$$\begin{aligned} \frac{\bar{s}\bar{s}\bar{d}}{\bar{s}\bar{u}\bar{d}} &= \frac{\Xi^- + 0.5\Xi^*(1530)}{\bar{\Lambda} + \bar{\Sigma}^0 + 0.92\bar{\Sigma}^*(1385)}, & \frac{ssd}{sud} &= \frac{\Xi^- + 0.5\Xi^*(1530)}{\Lambda + \Sigma^0 + 0.92\Sigma^*(1385)}, \\ \frac{\bar{s}\bar{s}\bar{d} + ssd}{\bar{s}\bar{u}\bar{d} + sud} &= \frac{\Xi^- + 0.5\Xi^*(1530) + \Xi^- + 0.5\Xi^*(1530)}{\bar{\Lambda} + \bar{\Sigma}^0 + 0.92\bar{\Sigma}^*(1385) + \Lambda + \Sigma^0 + 0.92\Sigma^*(1385)}. \end{aligned}$$

Above, we have explicitly identified the main resonance contributions, accompanied by the appropriate branching ratio. Given their large spin-isospin quantum numbers, these resonances despite their greater mass are as important contributors to the final yields, as is the ground state. For the Λ , we also note the presence of inseparable $\Sigma^0 \rightarrow \Lambda + \gamma$ contribution.

It is practically impossible to separate decay contributions which dilute the intrinsic ratios ssd/sud , $\bar{s}\bar{s}\bar{d}/\bar{s}\bar{u}\bar{d}$ down to about 0.23 for the case of RHIC [31]. However, we see a clear enhancement (factor 3) over the $p-p$, $p-\bar{p}$ background for all A-A interactions here considered. Among these, the RHIC result is of most profound consequence as we shall address below, as it implies large excess of strangeness yield (compare figure 14). The enhancement of the antibaryon ratios seen in the $p-A$ ratio (middle field of figure 3) is *not* seen for baryons (see right field of figure 3). A simulated $p-A$ enhancement can arise from the annihilation of antihyperons produced by the reacting matter in the surrounding spectator nuclear matter. Namely, the annihilation cross section for singly strange hyperons is notably larger than for double strange hyperons. In consequence the $\bar{\Lambda}$ are more depleted than Ξ .

To avoid the semblance of $p-A$ enhancement process it is important to consider how the yield of individual hadrons behaves compared to expectations based on a cascade of N-N interactions. This view on the strange hadron enhancement has been presented by the CERN-SPS WA97 collaboration for 158A GeV Pb collisions with laboratory Pb target, and these results have been confirmed and extended in the more

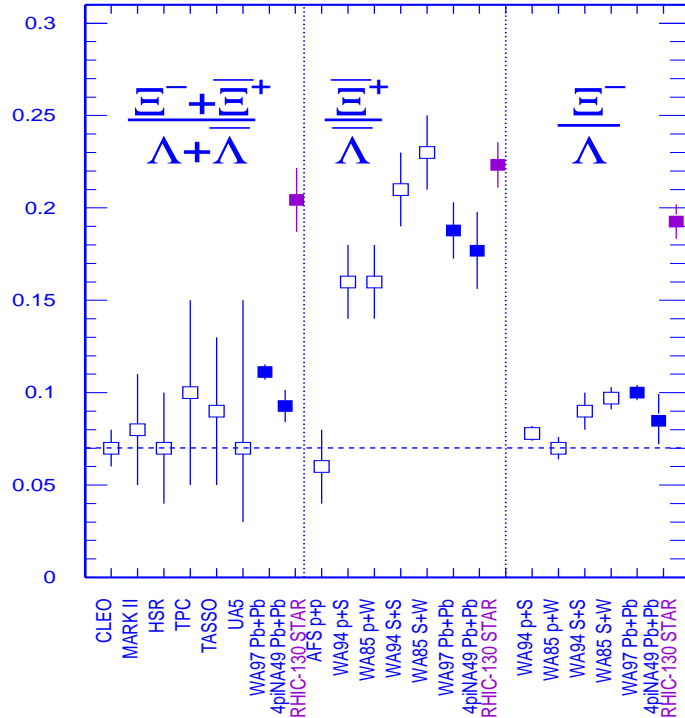


Figure 3. Ratios of hyperon abundances produced in high energy interactions. Recent experimental results from [27, 28, 29, 15, 6, 9, 30, 31].

recent NA57 measurements. In figure 4, we show the rise of the enhancement with the strangeness content, with p -Be reaction system used as reference. These results show yields per participant, where a participant is understood to be an inelastically reacting ‘wounded’ nucleon. These results confirm the QGP prediction of enhancement growth with a) strangeness b) antiquark content.

Before these studies of strangeness enhancement were carried out within the central rapidity region by NA57 and WA97 experiments, it has been shown that central rapidity is indeed the kinematic domain where the new physics is occurring. The NA35II experiment obtained $\bar{\Lambda}$ yield for 200A GeV Sulfur projectile on laboratory Sulfur target [32, 33]. As can be seen in figure 5, the antibaryon yields are localized in the central CM (center of momentum) rapidity region. The background p - p production result, shown by squares is obtained scaling up the yield by the number of nucleon participants. We see that the central rapidity is in fact the domain of the large enhancement as would be expected in a reaction picture in which a fireball of hot matter is formed.

Strangeness yield as function of rapidity is obtained evaluating $\langle s + \bar{s} \rangle = 1.6\Lambda + 1.6\bar{\Lambda} + 4K_S$, and is seen in figure 6. Again, the measured result is reflected at CM rapidity and the squares provide a hadron multiplicity scaled p - p result as basis. Thus, the enhancement, seen in figure 6, is expressing how much *faster* than nonstrange hadron strangeness increases in S-S interactions compared to p - p .

One would expect naively, in such a comparison, a reduction rather than an enhancement, since in a cascade of conventional hadronic reactions, it would be easier

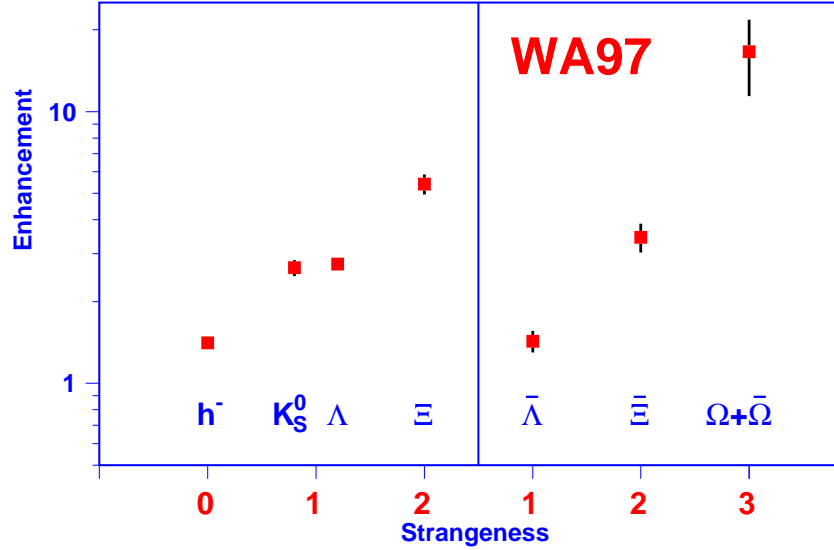


Figure 4. Abundance enhancement with respect to the yield in p-Be collisions, scaled with the number of ‘wounded’ nucleons, results of the WA97 collaboration [13].

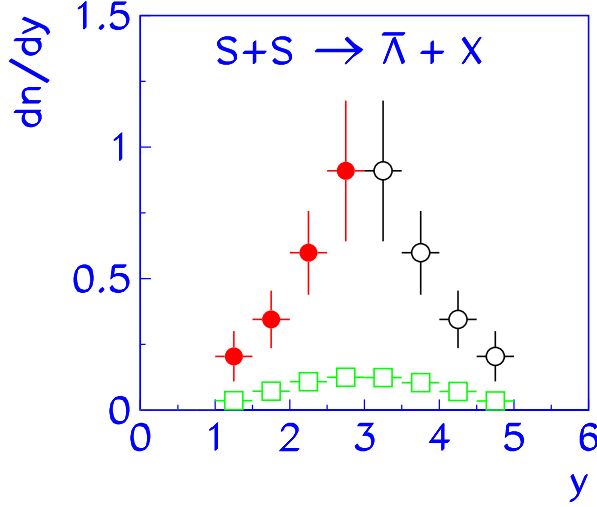


Figure 5. $\bar{\Lambda}$, in NA35II 200A GeV S-S interactions [32]. Background (squares) from multiplicity scaled N-N reactions forward (open circles) points: reflection at the CM rapidity.

to produce less massive pions, than strangeness, remembering that cascading hadrons degrade in energy. There can be no doubt seeing this result that even in the relatively small S-S reaction system there is a new physical mechanism of strangeness production at work. In absolute number, the yield of strangeness, seen in figure 6, is rather large, above 25 $s\bar{s}$ pairs. Our predictions that this could be happening should QGP phase be formed were classified 20 years ago at the LBL Heavy Ions Studies among ‘exotica’.

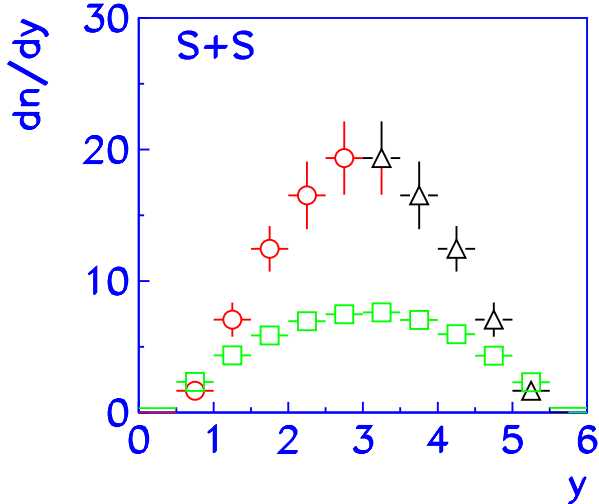


Figure 6. CM-rapidity reflected $1.6\Lambda + 1.6\bar{\Lambda} + 4K_S$ 200A GeV S-S multiplicity scaled 200A GeV $p-p$ results drawn from NA35II experiment [33].

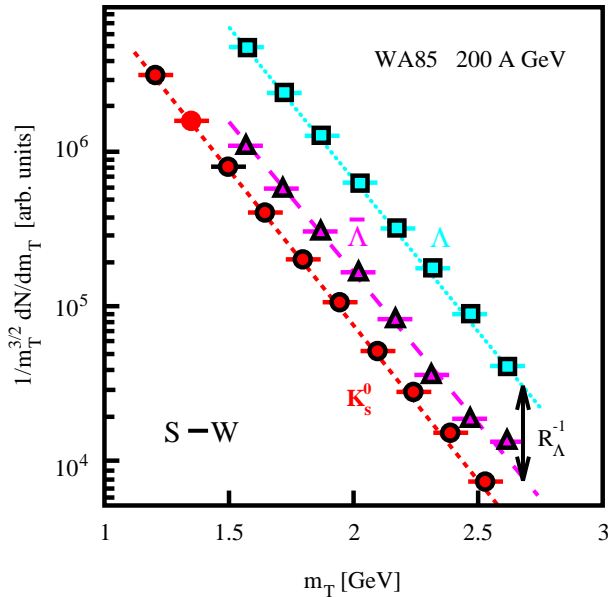


Figure 7. Central rapidity spectra of single strange K_S , Λ and $\bar{\Lambda}$ reported by the experiment WA85 [34]. Antibaryon to baryon ratio $R_\Lambda \equiv \bar{\Lambda}/\Lambda$ is independent of m_\perp .

Aside of particle yields, an important further key piece of physical evidence is the shape of transverse mass $m_\perp = \sqrt{m^2 + p_\perp^2}$ spectra. The experimental results cannot be understood within a conventional hadron cascade reaction picture. When the (central rapidity) m_\perp spectral distributions are fitted to an exponential shape, one finds that the inverse m_\perp slopes show a rather precise baryon-antibaryon universality, even though at CERN-SPS significant baryon number asymmetry prevails. This was

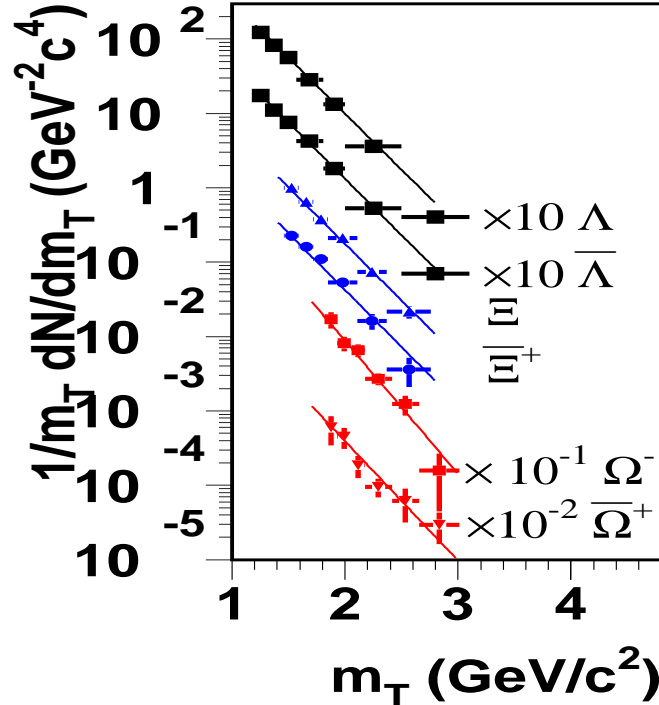


Figure 8. Central rapidity spectra of strange baryons Λ (*sud*), Ξ^- (*ssd*), Ω (*sss*) and their antibaryons $\bar{\Lambda}$, $\bar{\Xi}$, $\bar{\Omega}$ reported by the experiment WA97 [35].

first discovered in S-induced collisions by WA85 experiment [34], see figure 7. This is confirmed by the WA97 experiment in Pb–Pb Interactions [35], see figure 8, with the slopes given in table 1. The inverse slopes of the baryon and antibaryon spectra are to a very great precision (1%) the same. Also, within the error, the slopes of Λ and Ξ are the same. Results of the experiment NA57 indicate that the more precisely measured Ω and $\bar{\Omega}$ spectra are also yielding the same T_\perp . We understand the kaon-hyperon slope difference to be result of the collective explosive flow [36], and the different range of m_\perp considered evaluating the m_\perp slopes.

These m_\perp -slope results, found in different reaction systems, cannot be accidental, also since a different pattern of behavior is clearly seen in p – p and p – A reactions. The identity of baryon and antibaryon m_\perp slopes observed in A – A reactions prove that strange baryons and antibaryons are produced by the same mechanism in nuclear collisions, and do not suffer rescattering in a dense baryon-rich medium after their production. A systematic experimental [35] and theoretical [37] study of the m_\perp spectra for the central rapidity Pb–Pb reactions at projectile energy $158A$ GeV as function of reaction centrality confirms that Kaons and strange hyperons and antihyperons are born simultaneously and do not undergo rescattering. To the best of our understanding the only physical mechanism which can lead to this result is a QGP fireball breakup into free streaming hadrons, as would be expected in sudden hadronization of a QGP fireball [38, 39, 40, 41].

In figure 9, we show a survey of the SPS-158A GeV transverse slopes. The inverse slope parameter T is related to the intrinsic thermal parameters T_{tf} in the source and

Table 1. The inverse slope T_{\perp} of m_{\perp} spectra seen in figure 8, Pb–Pb interactions at 158A GeV, WA97 experiment [35].

Particle	K_S	Λ	$\bar{\Lambda}$	Ξ	$\bar{\Xi}$	$\Omega + \bar{\Omega}$
T_{\perp} [MeV]	230 ± 2	289 ± 3	287 ± 4	286 ± 9	284 ± 17	251 ± 19

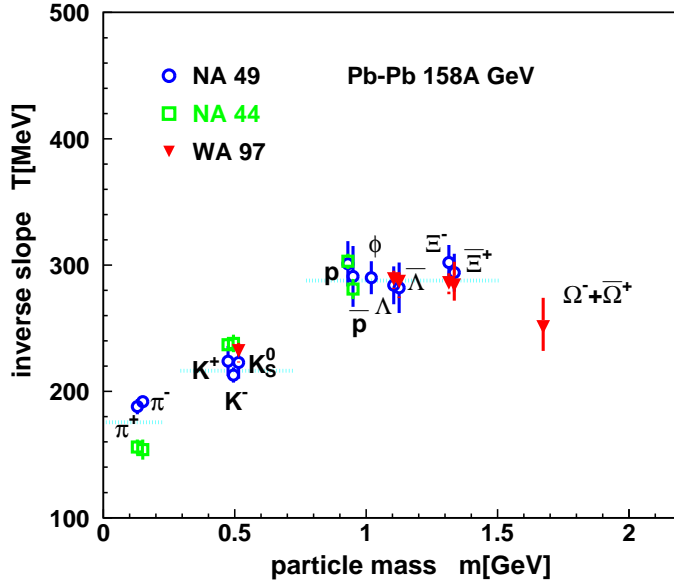


Figure 9. Inverse slopes of particle spectra obtained for Pb–Pb interactions at projectile energy 158A GeV.

local flow velocity v_{tf} , for $m, p_{\perp} \gg T$ by the usual Doppler formula :

$$T \simeq \frac{1 + \vec{n} \cdot \vec{v}_{\text{tf}}}{\sqrt{1 - \vec{v}_{\text{tf}}^2}} T_{\text{tf}} \rightarrow \sqrt{\frac{1 + v_{\text{tf}}}{1 - v_{\text{tf}}}} T_{\text{tf}}. \quad (2)$$

3. Kinetic description of strangeness production in QGP

We view a QGP fireball as consisting of quarks and gluons constrained by the external ‘frozen color vacuum’. Within the deconfined domain these particles can move and undergo collisions, and reactions, within a volume much larger than the usual nucleon size. The reactions occur at energies characterized by thermal equilibrium and thus the kinetic process like this is often called ‘thermal production’ in order to distinguish these soft reactions from hard kinetic processes occurring prior to thermalization of the incoming particle momenta. These first collision processes play a decisive role in providing abundance of charm, and heavier flavors, in quark–gluon plasma.

However, ‘thermal production’ can mean something entirely different in other related work. Namely, this term has also been used to describe the statistical yield of particles in chemical equilibrium. Both usages coincide only when the dynamics of the reaction process allows for the kinetic processes to establish chemical equilibrium. This, in general, will not be the case in heavy ion collisions at relativistic energies.

The generic angle averaged cross sections for (heavy) flavor s, \bar{s} production processes $g + g \rightarrow s + \bar{s}$ and $q + \bar{q} \rightarrow s + \bar{s}$, in lowest order are well known:

$$\bar{\sigma}_{gg \rightarrow s\bar{s}}(s) = \frac{2\pi\alpha_s^2}{3s} \left[\left(1 + \frac{4m_s^2}{s} + \frac{m_s^4}{s^2} \right) \tanh^{-1} W(s) - \left(\frac{7}{8} + \frac{31m_s^2}{8s} \right) W(s) \right], \quad (3)$$

$$\bar{\sigma}_{q\bar{q} \rightarrow s\bar{s}}(s) = \frac{8\pi\alpha_s^2}{27s} \left(1 + \frac{2m_s^2}{s} \right) W(s). \quad W(s) = \sqrt{1 - 4m_s^2/s} \quad (4)$$

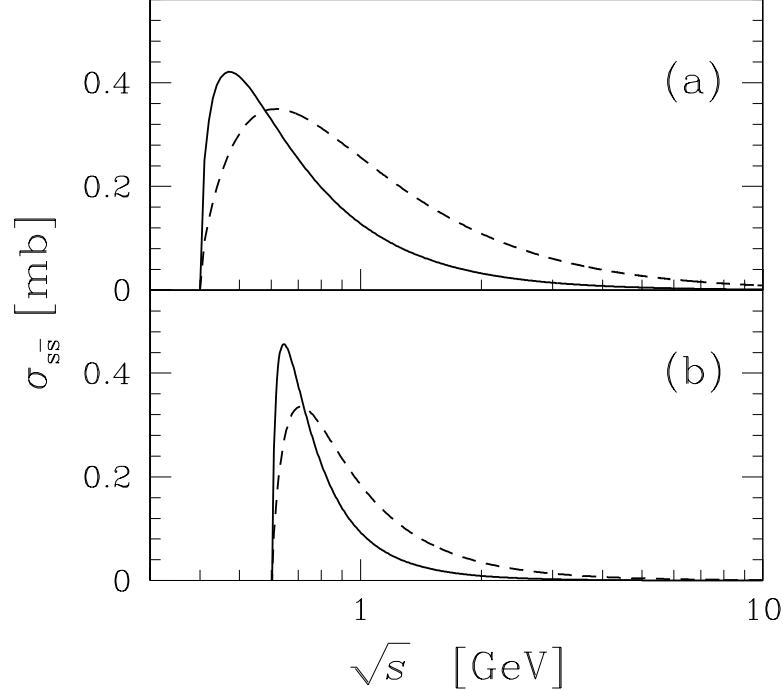


Figure 10. QGP strangeness production cross sections [3]: Solid lines $q\bar{q} \rightarrow s\bar{s}$; dashed lines $gg \rightarrow s\bar{s}$. a) for fixed $\alpha_s = 0.6$, $m_s = 200$ MeV; b) for running $\alpha_s(\sqrt{s})$ and $m_s(\sqrt{s})$, with $\alpha_s(M_Z) = 0.118$. $m_s(M_Z) = 90$ MeV, $m_s(1\text{GeV}) \simeq 2.1m_s(M_Z) \simeq 200$ MeV.

Considering that the kinetic (momentum) equilibration is faster than the process of strangeness production (chemical equilibration), we use equilibrium Fermi-Dirac or Bose particle distributions $f(\vec{p}_i, T)$ to obtain the thermally averaged strangeness production rate:

$$\langle \sigma v_{\text{rel}} \rangle_T \equiv \frac{\int d^3p_1 \int d^3p_2 \sigma_{12} v_{12} f(\vec{p}_1, T) f(\vec{p}_2, T)}{\int d^3p_1 \int d^3p_2 f(\vec{p}_1, T) f(\vec{p}_2, T)}. \quad (5)$$

This leads to the (Lorentz invariant) reaction rate per unit volume and time:

$$A^{gg \rightarrow s\bar{s}} = \frac{1}{2} \rho_g^2(t) \langle \sigma v \rangle_T^{gg \rightarrow s\bar{s}}, \quad A^{q\bar{q} \rightarrow s\bar{s}} = \rho_q(t) \rho_{\bar{q}}(t) \langle \sigma v \rangle_T^{q\bar{q} \rightarrow s\bar{s}}, \quad (6)$$

$$A^{s\bar{s} \rightarrow gg, q\bar{q}} = \rho_s(t) \rho_{\bar{s}}(t) \langle \sigma v \rangle_T^{s\bar{s} \rightarrow gg, q\bar{q}}.$$

The factor $1/2$, introduced here for two gluon processes, compensates the double-counting of identical particle pairs, arising since we are averaging considering all

reacting particles and thus each pair is counted twice. This invariant rate equation (6) is the source term for the strangeness current:

$$\partial_\mu j_s^\mu \equiv \frac{\partial \rho_s}{\partial t} + \frac{\partial \vec{v} \rho_s}{\partial \vec{x}} = A^{gg \rightarrow s\bar{s}} + A^{q\bar{q} \rightarrow s\bar{s}} - A^{s\bar{s} \rightarrow gg, q\bar{q}}. \quad (7)$$

In the local rest frame of reference ($\vec{v} = 0$) and ignoring the collective flow of matter we have:

$$\frac{d\rho_s}{dt} = \frac{d\rho_{\bar{s}}}{dt} = \frac{1}{2} \rho_g^2(t) \langle \sigma v \rangle_T^{gg \rightarrow s\bar{s}} + \rho_q(t) \rho_{\bar{q}}(t) \langle \sigma v \rangle_T^{q\bar{q} \rightarrow s\bar{s}} - \rho_s(t) \rho_{\bar{s}}(t) \langle \sigma v \rangle_T^{s\bar{s} \rightarrow gg, q\bar{q}}. \quad (8)$$

Evolution for s and \bar{s} is identical, which allows to set $\rho_s(t) = \rho_{\bar{s}}(t)$. Using detailed balance to simplify, we obtain:

$$\frac{d\rho_s}{dt} = A \left(1 - \frac{\rho_s^2(t)}{\rho_s^2(\infty)} \right), \quad A = A^{gg \rightarrow s\bar{s}} + A^{q\bar{q} \rightarrow s\bar{s}}. \quad (9)$$

The generic solution at fixed T ($\rho \propto \tanh(t/2\tau_s)$) implies that in all general cases there is an exponential approach to chemical equilibrium

$$\frac{\rho_s(t)}{\rho_s^\infty} \rightarrow 1 - e^{-t/\tau_s} \quad \tau_s \equiv \frac{1}{2} \frac{\rho_s(\infty)}{\frac{1}{2} \rho_g^2(t) \langle \sigma v \rangle_T^{gg \rightarrow s\bar{s}} + \rho_q(t) \rho_{\bar{q}}(t) \langle \sigma v \rangle_T^{q\bar{q} \rightarrow s\bar{s}} + \dots}, \quad (10)$$

where the characteristic time constant τ_s is the ratio of the density we are ‘chasing’ with the rate at which the case occurs. There could be additional strangeness formation processes as is suggested in equation (10) in denominator for τ_s .

The strangeness chemical relaxation time is rather short, evaluation of the diverse expressions presented here produces the result seen in figure 11, where the large uncertainty is due to 20% uncertainty in the value of the strange quark mass. We recognize that the standard QCD cross sections $\sigma_{\text{QCD}}^{gg \rightarrow s\bar{s}}$ and particle densities associated with a temperature $T > 200$ MeV yield τ_s similar to lifespan of the plasma phase. Here, we note that both τ_s and the lifespan of plasma decrease with increasing temperature of the initial state: for the plasma lifespan this is due to more explosive outflow of matter driven by greater initial pressure, while for τ_s this behavior is result of both the increased particle density and increased average reaction energy.

The temporal evolution of the strangeness density can be arrived at considering entropy conserving expansion $T^3 V = \text{Const.}$ and allowing for the dilution of the strange quark density by collective matter flow. Introducing the phase space occupancy factor γ_s^{QGP} and limiting ourselves to consider Boltzmann distribution, we find that γ_s^{QGP} evolves in time according to:

$$2\tau_s \frac{dT}{dt} \left(\frac{d\gamma_s^{\text{QGP}}}{dT} + \frac{\gamma_s^{\text{QGP}}}{T} z \frac{K_1(z)}{K_2(z)} \right) = 1 - (\gamma_s^{\text{QGP}})^2, \quad \gamma_s^{\text{QGP}}(t) \equiv \frac{n_s^{\text{QGP}}(t)}{n_s^\infty}, \quad z = \frac{m_s}{T}. \quad (11)$$

where K_i are the Bessel functions. We see that the time dependence of temperature determines the scale at which γ_s^{QGP} evolves. Solutions of this equation show that one can oversaturate the final QGP phase space, since the large initial strangeness abundance, even if sub-equilibrium at that time, can exceed the equilibrium population at lower temperature [20].

The same methods can be applied in the study of thermal charm formation. The relaxation time constant seen in figure 12 is large, indicating that charm will not be significantly produced in thermal parton collisions. On the other hand, charm is produced abundantly in first hard parton collisions. Benchmark values are 10 $c\bar{c}$ pairs in central Au–Au at RHIC-200; and 200 $c\bar{c}$ pairs in central Pb–Pb LHC-6000 reactions [42]. This yield is greater than the expected equilibrium yield at hadronization of QGP.

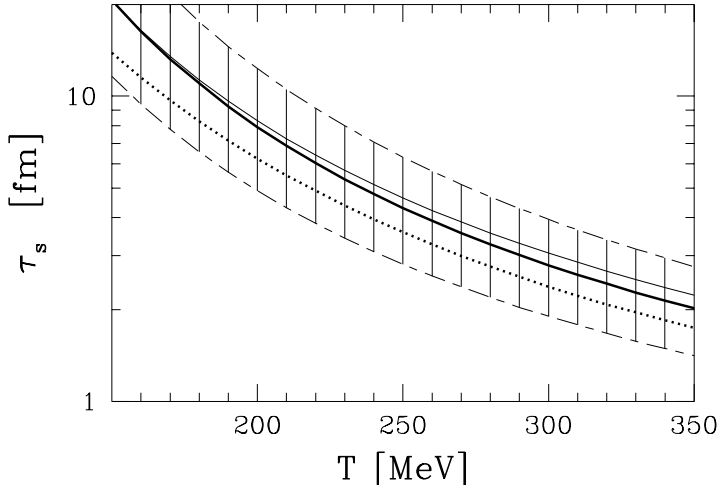


Figure 11. Strangeness thermal relaxation time constant as function of temperature. Dotted line is for fixed $\alpha_s = 0.6$ and $m_s = 200$ MeV while the solid lines are for running QCD parameters, see figure 10(b). Thin solid line indicates the remaining uncertainty in α_s while the hatched area indicates the domain for 20% variation of m_s .

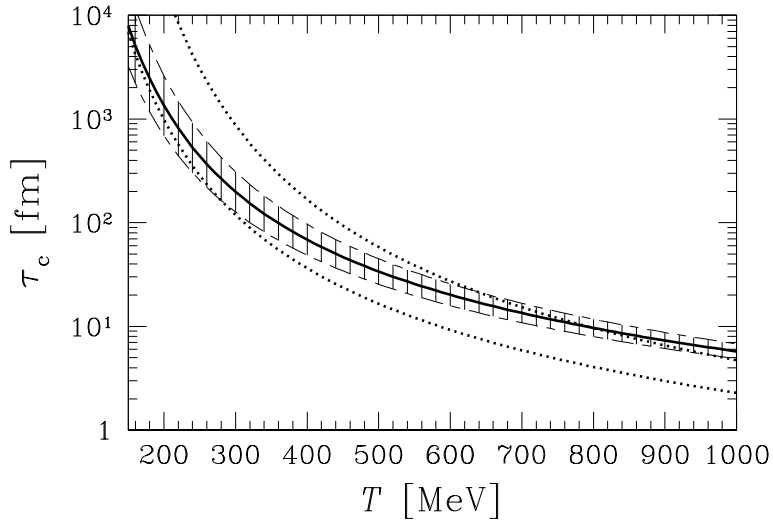


Figure 12. Charm thermal relaxation time constant obtained for $\alpha_s(M_Z) = 0.118$, $m_c(M_Z) = 0.7 \pm 7\%$ GeV.

4. Statistical hadronization

Hadron production is well described in a large range of yields by the mechanism of statistical hadronization [43]. This approach works in high energy nuclear collisions far better than has been anticipated by Fermi [44], the inventor of this method. An important result of statistical hadronization is that within a particle ‘family’, particle yields with same valance quark content are in relation to each other thermally equilibrated, e.g., the relative yield of $\Delta(1230)(qqq)$ and $N(qqq)$ or $K^*(\bar{s}q)$ and $K(\bar{s}q)$

Table 2. Four quarks: $s, \bar{s}, q, \bar{q} \rightarrow$ four chemical parameters.

γ_i	controls overall abundance of quark ($i = q, s$) pairs	Absolute chemical equilibrium
λ_i	controls difference between strange and non-strange quarks ($i = q, s$)	Relative chemical equilibrium

are completely controlled by the particle masses m_i , statistical weights (degeneracy) g_i and the hadronization temperature T . In the Boltzmann limit one has:

$$\frac{n^*}{n} = \frac{g^* m^* {}^2 K_2(m^*/T)}{g m^2 K_2(m/T)}. \quad (12)$$

Measurement of hadron resonances can thus sensitively test the statistical hadronization hypothesis. Since it is possible that the decay products of resonances rescatter, in principle not all resonances can be reconstructed by the invariant mass method. Thus, one expects that the experimental result must be below the ratio equation (12) expected for a given temperature. This will be the case for our study of K^*/K and $\Lambda(1520)/\Lambda$ for which the data is available. In fact, in our study of particle yields in section 5, the experimental ratio [45, 46, 47]: $(K^* + \bar{K}^*)/K^- = 0.26 \pm 0.07$. We find that this result is exactly in agreement with our hadronization temperature, $T = 145$ MeV, see table 3. We also find $\Lambda(1520)/\Lambda = 0.053$ which is about twice as large as the experimental value [48]: 0.025 ± 0.07 . This reduced experimental yield confirms that d-wave resonance $\Lambda(1520)$ is particularly fragile in matter [49].

The yields of particles are aside of temperature also controlled by their fugacity $\Upsilon_i \equiv e^{\sigma_i/T}$, where σ_i is particle ‘i’ chemical potential. Since for each related particle and antiparticle pair we need two chemical potentials, it has become convenient to choose parameters such that we can control the difference and sum of these separately. For example for nucleons and antinucleons N, \bar{N} the two chemical factors are chosen as:

$$\sigma_N \equiv \mu_b + T \ln \gamma_N, \quad \sigma_{\bar{N}} \equiv -\mu_b + T \ln \gamma_{\bar{N}}, \quad (13)$$

$$\Upsilon_N = \gamma_N e^{\mu_b/T}, \quad \Upsilon_{\bar{N}} = \gamma_{\bar{N}} e^{-\mu_b/T}. \quad (14)$$

The role of the two factors can be understood considering at the first law of thermodynamics:

$$\begin{aligned} dE + P dV - T dS &= \sigma_N dN + \sigma_{\bar{N}} d\bar{N}, \\ &= \mu_b (dN - d\bar{N}) + T \ln \gamma_N (dN + d\bar{N}). \end{aligned}$$

The (baryo)chemical potential μ_b , controls the baryon number, arising from the particle difference. γ , the phase space occupancy, regulates the number of nucleon–antinucleon pairs present. At the quark level (combining the light quarks u, d in one q , we have the situation shown in table 2.

There is considerable difference how the two types of chemical factors influence particle yield equilibration. This is best understood considering strangeness in the hadronic gas phase, the two principal chemical processes are seen in figure 13. The redistribution of strangeness among (in this example) Λ, π and N, K constitutes approach to the relative chemical equilibrium of these species. The production processes, on right in figure 13, are responsible for absolute chemical equilibrium of strangeness. Achievement of the absolute equilibrium, $\gamma \rightarrow 1$, require more rarely

occurring truly inelastic collisions with creation of new particle pairs. These processes are absent in usual nonrelativistic chemical environments.

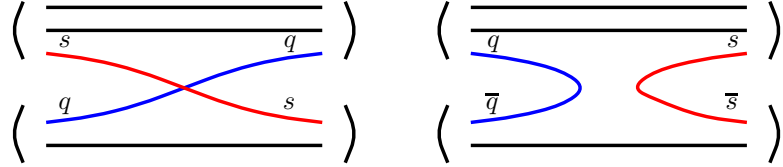


Figure 13. Typical strangeness exchange (left) and production (right) reactions in the hadronic gas phase.

When statistical hadronization of, e.g., a deconfined state of QGP occurs, the hadron yields are following closely the magnitude of the accessible phase space characterized by these chemical factors (and temperature). An important feature is the apparent under or over population of the resulting phase space. Namely, even if there is the pair abundance equilibrium in the primary QGP phase, in the secondary phase (here hadronic gas) phase space has different size in general. Absolute chemical equilibrium in the secondary phase requires a period of pair production accompanying hadronization. A long lasting QGP–HG mixed phase is today ruled out by experiment, and we should expect that the phase space occupancy chemical factors γ_i will be discontinuous at the phase transformation, and in general in the observed final state $\gamma_i \neq 1$.

There are many different hadrons, and in principle, we should assign to each a chemical potential and then look for chemical reactions which relate these chemical potentials, e.g., on left in figure 13, we infer $\mu_\Lambda + \mu_\pi = \mu_N + \mu_K$. However, more direct way to accomplish the same objective consists in characterizing each particle by the valance quark content [50], forming a product of chemical factors, e.g., for $p(uud)$,

$$\Upsilon_{p(uud)} = \gamma_u^2 \gamma_d \lambda_u^2 \lambda_d, \quad \Upsilon_{\bar{p}(\bar{u}\bar{u}\bar{d})} = \gamma_u^2 \gamma_d \lambda_u^{-2} \lambda_d^{-1},$$

note here that:

$$\lambda_i = e^{\mu_i/T}, \quad \mu_q = \frac{1}{2}(\mu_u + \mu_d), \quad \lambda_q^2 = \lambda_u \lambda_d \quad \lambda_b = \lambda_q^3.$$

This implies relations between quark based $\mu_i, i = u, d, s$ and hadron based $\mu_i, i = b, S$ chemical potentials:

$$\mu_b = 3\mu_q, \quad \mu_s = \frac{1}{3}\mu_b - \mu_S, \quad \lambda_s = \frac{\lambda_q}{\lambda_S},$$

An important anomaly is the historically negative S-strangeness in s -hadrons. e.g.:

$$\begin{aligned} \Upsilon_\Lambda &= \gamma_u \gamma_d \gamma_s e^{(\mu_u + \mu_d + \mu_s)/T} = \gamma_u \gamma_d \gamma_s e^{(\mu_b - \mu_S)/T}, \\ \Upsilon_{\bar{\Lambda}} &= \gamma_u \gamma_d \gamma_s e^{(-\mu_u - \mu_d - \mu_s)/T} = \gamma_u \gamma_d \gamma_s e^{(-\mu_b + \mu_S)/T}. \end{aligned}$$

The phase space density is:

$$\frac{d^6 N_i}{d^3 p d^3 x} = g_i \frac{\Upsilon_i}{(2\pi)^3} e^{-E_i/T}, \quad (15)$$

$$\frac{d^6 N_i^{\text{F/B}}}{d^3 p d^3 x} = \frac{g_i}{(2\pi)^3} \frac{1}{\Upsilon_i^{-1} e^{E_i/T} \pm 1}, \quad \Upsilon_i^{\text{bosons}} \leq e^{m_i/T}. \quad (16)$$

and thus the 4π particle yield is proportional to the phase space integral, for example for π , N and \overline{N} :

$$\frac{N_\pi}{V} = C g_\pi \int \frac{d^3 p}{(2\pi)^3} \frac{1}{\gamma_q^{-2} e^{\sqrt{m_\pi^2 + p^2}/T} - 1}, \quad \gamma_q^2 < e^{m_\pi/T} \simeq (1.6)^2,$$

$$\frac{N}{V} = C g_N \int \frac{d^3 p}{(2\pi)^3} \frac{1}{1 + \gamma_q^{-3} \lambda_q^{-3} e^{E/T}}, \quad \frac{\overline{N}}{V} = C g_N \int \frac{d^3 p}{(2\pi)^3} \frac{1}{1 + \gamma_q^{-3} \lambda_q^{+3} e^{E/T}}.$$

One can show that there is no influence of matter flow dynamics on this complete ‘ 4π ’ particle yield.

When a small region of rapidity is considered, but the yield of particles is practically constant as function of rapidity, it is possible to imagine that the yield arise from a series of fireballs placed at different rapidities, and thus in this limit we also can proceed as if we had a full phase space integral. However, the proportionality constant C is, in this case in particular, but also more generally for a dynamically evolving system, not the system volume. We recall that though the individual phase space integrals are easily evaluated, to get the full yield one has to be sure to include all the hadronic particle decays feeding into the yield considered, e.g., the decay $K^* \rightarrow K + \pi$ feeds into K and π yields. This actually constitutes a book keeping challenge in study of particle multiplicities, since decays are contributing at the 50% level to practically all particle yields, sometimes the decay contribution can be dominant, as is generally the case for the pion yield, yet each resonance contributes relatively little in the final count, it is the large number of resonances that matters.

It is often more appropriate to study ratios of particle yields as these can be chosen such that certain physical features can be isolated. For example, just the two ratios

$$R_\Lambda = \frac{\overline{\Lambda} + \overline{\Sigma}^0 + \overline{\Sigma}^* + \dots}{\Lambda + \Sigma^0 + \Sigma^* + \dots} = \frac{\bar{s}\bar{q}\bar{q}}{sqq} = \lambda_s^{-2} \lambda_q^{-4} = e^{2\mu_s/T} e^{-2\mu_b/T},$$

$$R_\Xi = \frac{\overline{\Xi}^- + \overline{\Xi}^* + \dots}{\Xi^- + \Xi^* + \dots} = \frac{\bar{s}\bar{s}\bar{q}}{sqq} = \lambda_s^{-4} \lambda_q^{-2} = e^{4\mu_s/T} e^{-2\mu_b/T},$$

lead to a very good estimate of the baryochemical potential and strange chemical potential [38], and thus to predictions of other particle ratios. The sensitivity to phase space occupancy factors γ_i derives from comparison of hadron yields with differing q, s quark content, e.g.:

$$\frac{\Xi^-(dss)}{\Lambda(dds)} \propto \frac{\gamma_d \gamma_s^2}{\gamma_d^2 \gamma_s} \frac{g_\Xi \lambda_d \lambda_s^2}{g_\Lambda \lambda_d^2 \lambda_s}, \quad \frac{\Xi^-(\bar{d}\bar{s}\bar{s})}{\Lambda(\bar{d}\bar{d}\bar{s})} \propto \frac{\gamma_d \gamma_s^2}{\gamma_d^2 \gamma_s} \frac{g_\Xi \lambda_d^{-1} \lambda_s^{-2}}{g_\Lambda \lambda_d^{-2} \lambda_s^{-1}}.$$

Note that $\gamma_q^2 \equiv \gamma_u \gamma_d$ and $\gamma_u \simeq \gamma_d$.

An interesting application arises when we consider product of the above ratios, as then the result depends on γ_s/γ_d and temperature. In figure 14, we see how this product of ratios shows for the RHIC₁₃₀ results that the equilibrium value $\gamma_s/\gamma_q = 1$ (where we set $\gamma_d \simeq \gamma_u \simeq \gamma_q$) is not compatible with the experimental results. Recall that the phase space occupancies we consider here are those arising from hadron yields and thus are applicable to the hadron yields, the excess above chemical equilibrium does not imply that the underlying state of, e.g., deconfined quark-gluon plasma is not chemically equilibrated.

It is at first hard to believe that the overpopulation of the strange quark phase space, as shown in figure 14, should be 50% grater than that of light quark phase

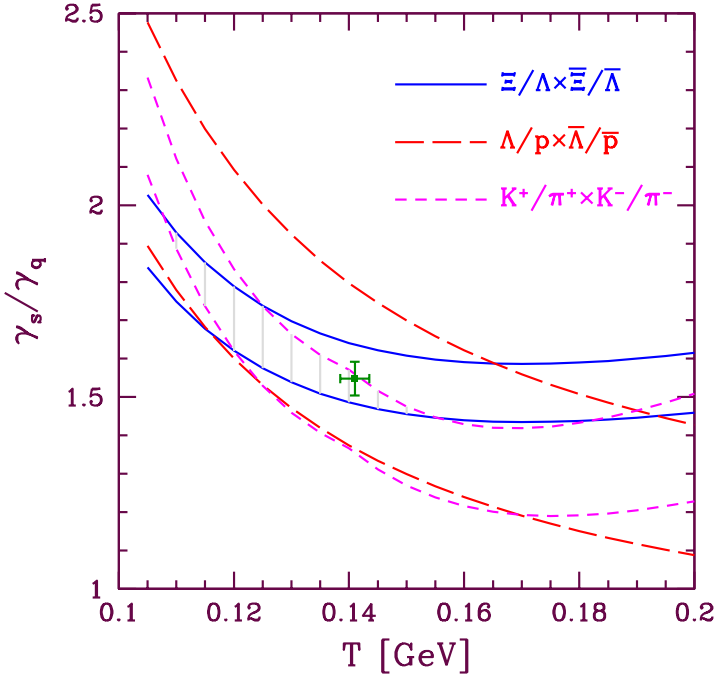


Figure 14. Evaluation of results of RHIC₁₃₀ experimental particle ratio results showing that $\gamma_s/\gamma_q > 1$ [5]. The cross is result of a global fit to all data, the bands reflect on the experimental uncertainty. Hatched area is the compatibility region for the three particle ratio products considered.

space. However, this should have been expected! As the kinetic theory of strangeness production presented in section 3 shows, the lower mass quarks approach equilibrium yield faster. Thus, while practically all QGP produced strange quark pairs escape to be observed, light quark pair can be more easily reequilibrated in their abundance. This argument assumes that the hadronization is not entirely sudden.

In the limit of very rapid hadronization, another mechanism favors abundance of strange quark pairs over light quark pairs in that there is a relatively small upper limit on γ_q . As there is no time to expand the volume, hadron formation has to absorb the high entropy content of QGP which originates in broken color bonds. As is seen in figure 15, the maximum entropy density S/V occurs for an oversaturated pion gas, $\gamma_q \simeq e^{m_\pi/2T} \simeq 1.6$. Just below this Bose condensation condition, the entropy density is twice as large as that of chemically equilibrated gas. The entropy content of a non-equilibrium Bose gas has to be evaluated recalling

$$S_\pi = \int \frac{d^3p d^3x}{(2\pi\hbar)^3} [(1 + f_\pi) \ln(1 + f_\pi) - f_\pi \ln f_\pi], \quad (17)$$

$$f_\pi(E) = \frac{1}{\gamma_q^{-2} e^{E_\pi/T} - 1}, \quad E_\pi = \sqrt{m_\pi^2 + p^2}. \quad (18)$$

We note that a similar constrain arising from kaon condensation limit yields the less restrictive condition:

$$\frac{\gamma_s}{\gamma_q} \left(\frac{\lambda_s}{\lambda_q} \right)^{\pm 1} < e^{(m_K - m_\pi)/T} \simeq 11. \quad (19)$$

We return to this interesting condition in section 7.

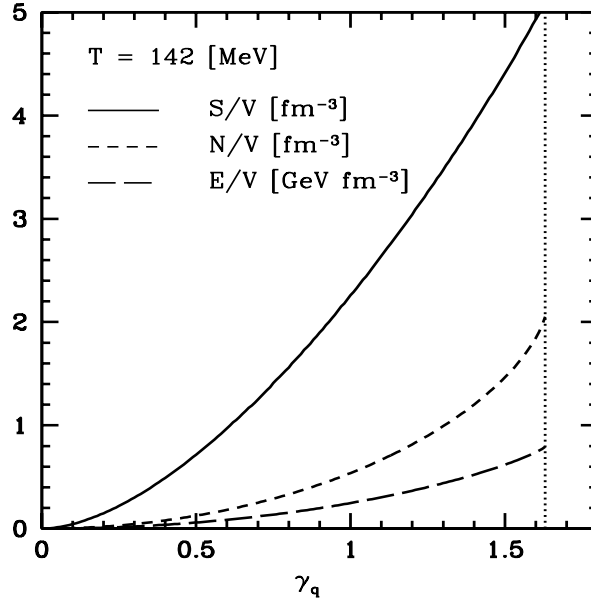


Figure 15. Entropy density S/V along with particle density N/V and energy density E/V for a non-equilibrium pion gas at $T = 142$ MeV.

5. Hadronization at SPS and RHIC

Given yields of (strange) hadrons, we can apply the principles described above to study the hadronization conditions, and we would like to do this here as function of energy. Experimental results were available to consider RHIC Au–Au collisions obtained at $\sqrt{s_{NN}^{CM}} = 130$ GeV and SPS Pb–Pb reactions at $\sqrt{s_{NN}^{CM}} = 8.75, 12.25, 17.2$ GeV (projectile energy $40A$ GeV, $80A$ GeV, $158A$ GeV), as well as S–Pb/W $200A$ GeV reactions occurring at $\sqrt{s_{NN}^{CM}} = 19.2$ GeV. The procedure we adopt is to fit statistical parameters for 4π particle multiplicity results. For SPS, the resulting χ^2/dof is shown in figure 16. The solid squares are obtained allowing 5 parameters, i.e., full chemical nonequilibrium, the open triangles assuming that complete chemical equilibrium prevails. Open square results were obtained assuming that light quarks are in chemical equilibrium. Except at $40A$ GeV, we find in our approach involving chemical nonequilibrium yields and only statistical errors, statistically very significant fits.

We use here SPS NA49 results [12], which include π^\pm , K , \bar{K} , Λ , $\bar{\Lambda}$, ϕ at $40, 80, 160A$ GeV and at top SPS energy, we find that the experimental results for Ξ , $\bar{\Xi}$, Ω , $\bar{\Omega}$ are reproduced nearly exactly even though for consistency we have not fitted these. Since this is a different data sample and we do not employ presently the central rapidity WA97 results, our fit result for some parameters will be slightly different, e.g., though we still report $\gamma_q^{\text{HG}} > 1$, the value we find is smaller than found using the complete data sample of NA49 and WA97.

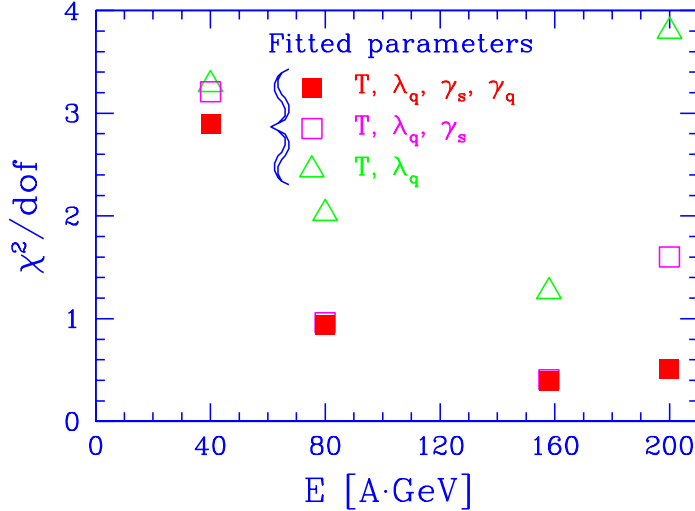


Figure 16. Quality of statistical hadronization fit to hadron yields: χ^2/dof for the 4 SPS reaction energies.

Table 3. Results of fit of RHIC₁₃₀ particle yields. Top line: statistical significance, following sections: fitted statistical parameters, hadro-chemical potentials, physical properties of the fireball. Stars indicate that a value is consequence of a constraint, and was not fitted.

RHIC ₁₃₀	non-equilibrium	equilibrium
χ^2/dof	27/(21 - 3)	230/(21 - 2)
T	144.6 ± 1.3	169.1 ± 2.3
λ_q	1.069 ± 0.008	1.067 ± 0.008
λ_s	1.0198^*	1.0167^*
γ_q^{HG}	1.62^*	1^*
$\gamma_s^{\text{HG}}/\gamma_q^{\text{HG}}$	1.53 ± 0.03	1^*
μ_b [MeV]	29.1	32.8
μ_s [MeV]	6.9	8.1
s/b	8.8	6.2
E/b [GeV]	32.8	31.8
S/b	215	218
E/S [MeV]	153	146
W_s	0.55	0.49

The RHIC fit favors non-equilibrium by such a large margin that we could not show the result on the same scale in figure 16. The actual values for χ^2/dof are seen in the top line of table 3. In obtaining these results it is assumed that 40% of weak decay cascades $\Xi \rightarrow \Lambda$ and $\Lambda \rightarrow p$ are accepted whenever such corrections were not applied to data by the experimental groups. In the chemical nonequilibrium fit, we assume that the maximum value of $\gamma_q = e^{m\pi/2T}$ is attained, and thus this value is not fitted. The value of λ_s is obtained from the requirement that strangeness balances,

$\langle s - \bar{s} \rangle = 0$. The other statistical parameter acquire values seen in table 3. We note that the hadronization temperature is greatly reduced in non-equilibrium approach compared to the value arrived at forcing chemical equilibrium. This is made possible by $\gamma_i > 1$, in this case the high particle yields seen at RHIC can be arrived at a lower value of hadronization temperature. We also present the hadron gas parameters μ_b, μ_S derived from λ_q, λ_s which can be used in back of envelope cross checks of expected particle ratios. These results constitute a slight update of our standard RHIC fit [5], where the actual particle multiplicities are also given.

Given the fitted set of statistical parameters (T, μ_i, γ_i) which characterize the phase space, we can evaluate, up to a common normalization constant, the strangeness $\langle s \rangle \simeq \langle \bar{s} \rangle$, energy E , baryon number b , entropy S contained by all produced hadronic particles, as shown in table 3. At the very bottom, we also present the Wróblewski ratio [51],

$$W_s = \frac{2\langle s\bar{s} \rangle}{\langle d\bar{d} + u\bar{u} \rangle}, \quad (20)$$

of newly produced strange quark pairs to all quark pairs. Strangeness production, while enhanced is not yet as abundantly produced as light flavors. We consider this ratio as function of \sqrt{s} in figure 17. The triangles for elementary $p-p$ reactions are consistent with ‘color string snapping’ process which yields strangeness pairs with about 22% abundance of the light quark pairs, and nearly independent of \sqrt{s} . In heavy ion collisions (circles), a much greater and \sqrt{s} dependent result is seen. This indicates that a new strangeness production process arises, which could well be the thermal production of strangeness in QGP. We also see, in the background, the results of a similar analysis obtained within the chemical semi-equilibrium approach [52].

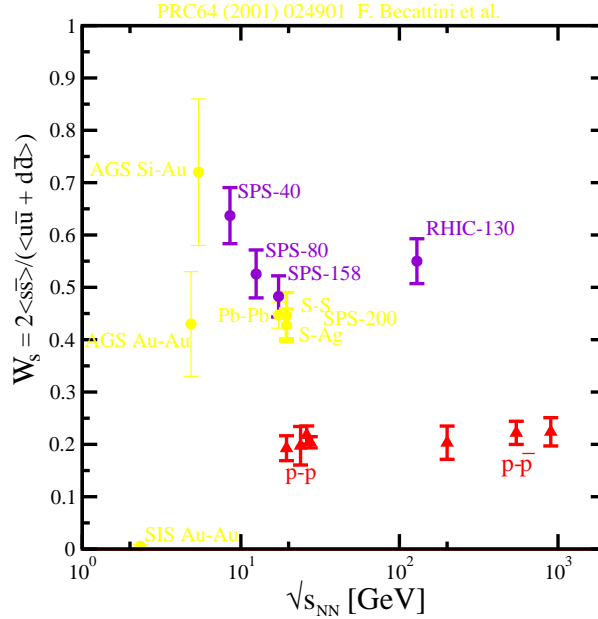


Figure 17. Wróblewski ratio [51] : only newly made s - and q -pairs are counted in comparing strange to light quark pair production.

The nonequilibrium parameters γ_s/γ_q , γ_q are displayed in figure 18. The results for γ_s/γ_q , on top, show that only at RHIC $\gamma_s > \gamma_q$. Open squares show that when

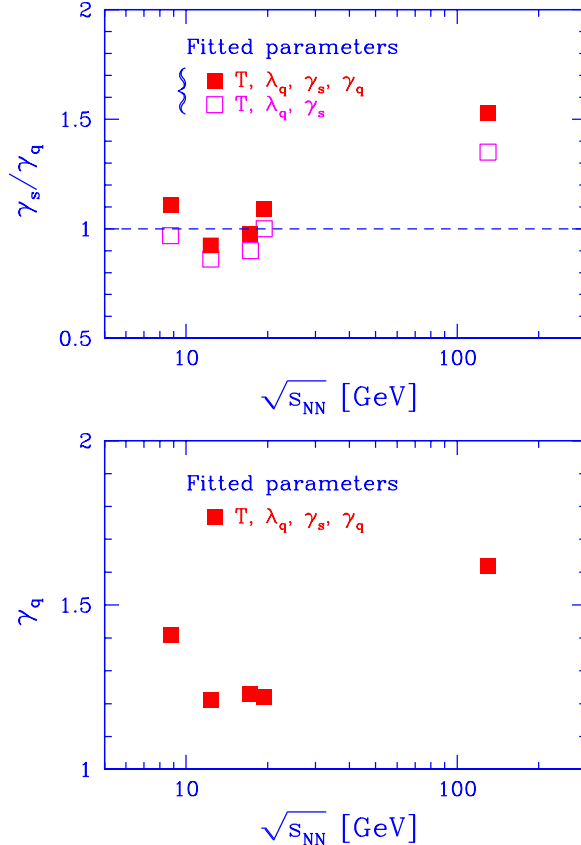


Figure 18. Fits of, top, γ_s/γ_q and, bottom, γ_q chemical nonequilibrium parameters as function of collision energy. Open squares results for $\gamma_q = 1$, in which case the left hand side gives γ_s .

we fix $\gamma_q = 1$ the SPS fits, in general, yield $\gamma_s < 1$, as is widely reported. However, bottom, we see that $\gamma_q > 1$ in all cases, reflecting on the excess in charged hadron multiplicity. We note that the 40A GeV SPS result (lowest energy point) deviates from the behavior systematics of the other results.

Since we know the incoming energy and we can evaluate the amount of thermal energy found in the final state hadrons, we have a good measure of the energy stopping for the different collision systems — to be precise in estimate of the energy stopping, we would have also to account for the energy transferred from intrinsic degrees of freedom to the collective flow. The behavior of the ratio of thermal energy to collision energy is seen in figure 19. The result is in so far surprising as energy stopping is somewhat greater at RHIC₁₃₀ than at top SPS energy. On the other hand, the rise of the energy stopping power towards lower SPS energies is expected, as is the steep rise for the asymmetric collision system S-Pb/W.

With the relatively great variability of stopping power seen in figure 19, it seems more prudent to use in study of energy dependence of different physical properties of the hot fireball not the collision energy but the final state thermal fireball energy content. This is strongly supported by the study of the systematics of strangeness production per baryon, seen in figure 20. On top, we show the strangeness excitation

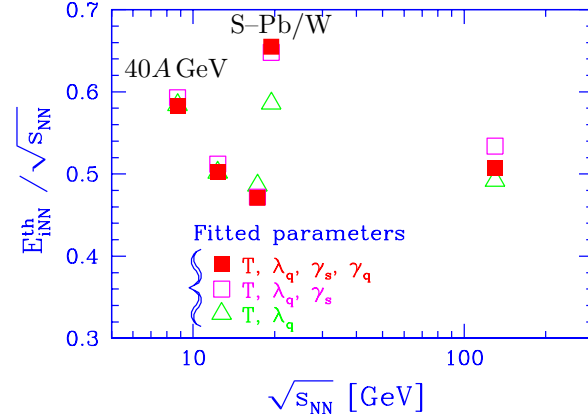


Figure 19. Fraction of energy stopping at SPS and RHIC: results are shown for 40, 80, 158A GeV Pb–Pb, 200A GeV S–W/Pb reactions and at RHIC for 65+65A GeV Au–Au interactions.

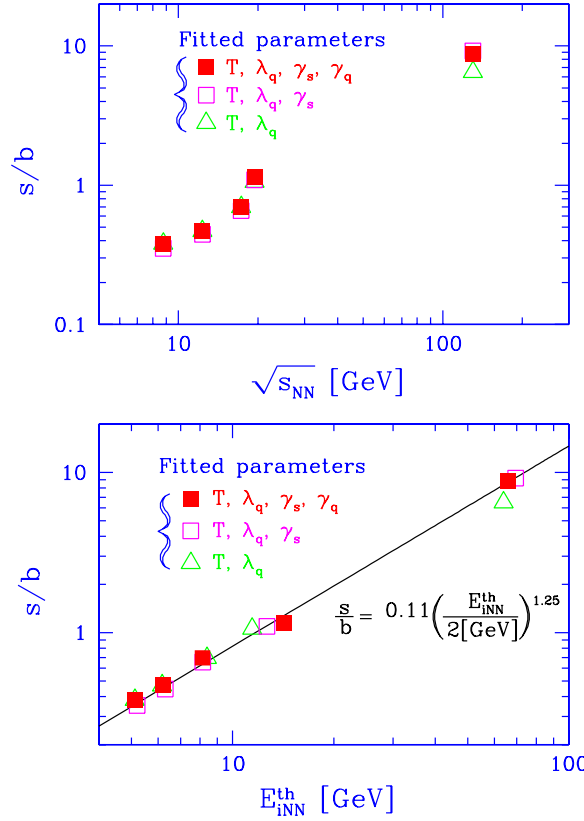


Figure 20. Strangeness per thermal baryon participant, top as function of $\sqrt{s_{NN}}$, bottom as function of E_{iNN}^{th} .

function as usually shown, using $\sqrt{s_{NN}}$ as variable, and normalizing to the baryon yield. The baryon number is conserved in hadronization, and this result is directly

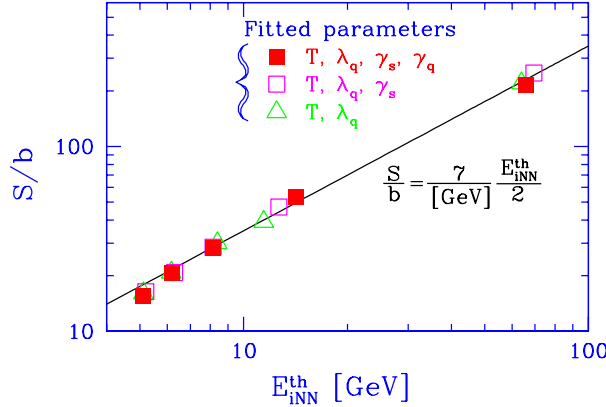


Figure 21. Entropy production per thermal participating thermal baryon S/b shown as function of the intrinsic thermal energy per baryon, E_{iNN}^{th} .

telling us how much strangeness was available prior to hadronization. We recall that the true ‘thermalized’ participants are about 5–10% fewer than is inferred from geometric consideration. On bottom in figure 20, we present the same result using as variable the intrinsic energy content. There is a significant simplification of the result and we find

$$\frac{s}{b} = 0.11 \left(\frac{E_{iNN}^{\text{th}}}{2[\text{GeV}]} \right)^{5/4}.$$

Importantly, there is no sign of a deviation of the systematics of strangeness production.

Similarly, considering the specific entropy content in figure 21, we find that entropy production per unit of available energy is universal:

$$\frac{S}{E_{iNN}^{\text{th}}} = \frac{7}{[\text{GeV}]}.$$

The entropy production mechanism which has this simple result for a wide range of intrinsic fireball energy is not known, but appears to be common for both SPS and RHIC energy range.

Comparing the results seen in figure 20 and figure 21, we note that, as function of the intrinsically available thermal energy, the strangeness production rises somewhat faster than entropy, which expresses the fact that strangeness is more enhanced than hadron multiplicity comparing RHIC to SPS. Within QGP phase, the strangeness to entropy ratio s/S , shown in figure 22, characterizes the approach to chemical equilibrium of strangeness, as compared to saturation of the availability of quarks and gluons. Both quantities may increase slightly in hadronization, but are expected to be practically conserved. Since the rise of s/S from SPS to RHIC is relatively slow, we show the behavior as function of both, top $\sqrt{s_{NN}}$, and bottom of E_{iNN}^{th} . There is clear increase of this ratio comparing SPS to RHIC, but the magnitude of the effect is somewhat dependent on the method of evaluation of chemical conditions.

There is perhaps an indication, in figure 22, of a possible increase of strangeness yield per entropy at the lowest energy, consistent with the somewhat anomalous rise of K^+/π^+ ratio reported by the NA49 experiment. Dynamically, this may be consequence of a longer lived QGP phase, which lacks the strength to undergo a

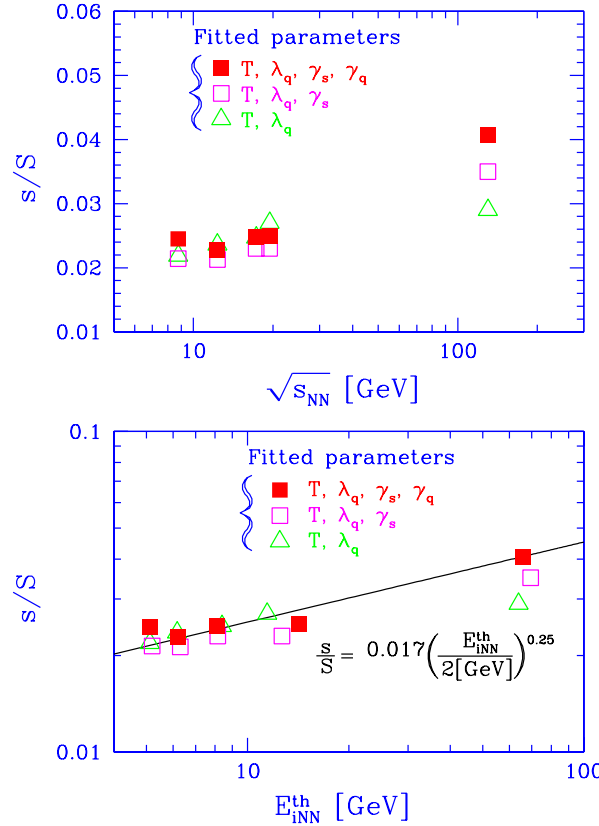


Figure 22. Strangeness per entropy: top as function of $\sqrt{s_{NN}}$, bottom as function of E_{iNN}^{th} .

fast collective flow. Longer lifespan even at lower initial temperature would help strangeness production. More systematic study of strangeness production in this energy range could thus offer significant insights into the properties of the deconfined phase. Ultimately, as the energy is reduced below the QGP threshold, there should be a significant cut in strangeness yield.

6. Onset of quark-gluon plasma formation

The properties of hot QCD matter can be well described in terms of a QGP model [53], which agrees with latest lattice results [54, 55, 56]. Thus, in principle, we understand the behavior of the QGP and can analyze the meaning of the relatively low hadronization temperatures. In figure 23, we show with solid squares the SPS and open square the RHIC hadronization points we obtained, dashed line corresponds to the cross over from the deconfined to confined phase. In the background, we see as triangles hadronization analysis for AGS and SIS assuming equilibrium conditions.

Our results are tabulated in table 4, obtained enforcing strangeness conservation (except for S-W) and allowing chemical nonequilibrium. As we go to press a fit at 30 GeV is still not possible, with particle yields not available. Statistical errors on the fit results are small and are not shown, in figure 23 we indicate our estimate

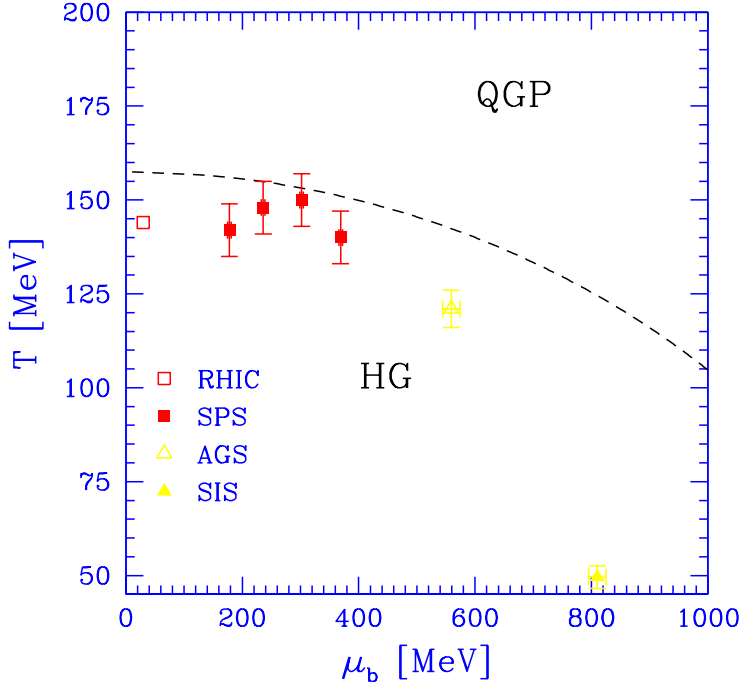


Figure 23. Hadronization conditions in T, μ_b plane: RHIC₁₃₀ open square, SPS solid squares.

Table 4. The results of nonequilibrium fits at SPS and RHIC: for each collision system we present the collision energy in laboratory, reaction energy $\sqrt{s_{NN}}$, the chemical freeze-out temperature T , and baryochemical potential μ_b ; these results are shown in figure 23. The bottom line gives the experimental ratio K/π , where available, see text for details.

	Au–Au	S–W	Pb–Pb	Pb–Pb	Pb–Pb	Pb–Pb
$\sqrt{E_{\text{lab}}}$ [GeV]	65+65	200	158	80	40	30
$\sqrt{s_{NN}}$ [GeV]	130	19.4	17.2	12.3	8.75	7.60
T [MeV]	144.6	143.5	148.5	150.3	139.5	–
μ_b [MeV]	30.1	165	236	302	370	–
K/π	0.16	–	0.12	0.11	0.11	0.12

of the systematic SPS result error based on 5% individual data point error. The relative changes between the fit results to NA49 40,80,158 GeV reactions are most likely significant, since the systematic error is common to these results. Thus it is the 80 GeV SPS hadronization point which is closest to the equilibrium phase transition between HG and QGP. The RHIC point (open square) though at low baryochemical potential could be at lower temperature than are the 160 GeV SPS and 80 GeV SPS results. The lowest temperature is found for the S–W point, but this result is obtained within a very different procedure, using central rapidity results of WA85 and a flow model. If at all, the temperature of hadronization seems to rise as the collision energy

falls, until we nearly touch the equilibrium phase transition condition. From thereon, we record a different behavior, with hadronization condition at 40 GeV moving more inward the hadron domain, with AGS and SPS equilibrium points deep within hadron gas phase.

To better understand this result, we must remember that the fireball is not a piece of deconfined matter sitting still. It undergoes a rather rapid collective explosive flow. Collective motion of color charged quarks and gluons contributes an important collective component in the pressure, as can be seen considering the stress portion of the energy-momentum tensor:

$$T^{ij} = P\delta_{ij} + (P + \varepsilon)\frac{v_i v_j}{1 - \vec{v}^2}. \quad (21)$$

The rate of momentum flow vector $\vec{\mathcal{P}}$ at the surface of the fireball is obtained from the energy-stress tensor T_{kl} :

$$\vec{\mathcal{P}} \equiv \hat{\mathcal{T}} \cdot \vec{n} = P\vec{n} + (P + \varepsilon)\frac{\vec{v}_c \vec{v}_c \cdot \vec{n}}{1 - \vec{v}_c^2}. \quad (22)$$

The pressure and energy comprise particle and the vacuum properties: $P = P_p - \mathcal{B}$, $\varepsilon = \varepsilon_p + \mathcal{B}$.

The condition $\vec{\mathcal{P}} = 0$ reads:

$$\mathcal{B}\vec{n} = P_p\vec{n} + (P_p + \varepsilon_p)\frac{\vec{v}_c \vec{v}_c \cdot \vec{n}}{1 - \vec{v}_c^2}. \quad (23)$$

Multiplying with \vec{n} , we find:

$$\mathcal{B} = P_p + (P_p + \varepsilon_p)\frac{\kappa v_c^2}{1 - v_c^2}, \quad \kappa = \frac{(\vec{v}_c \cdot \vec{n})^2}{v_c^2}. \quad (24)$$

This requires $P_p < \mathcal{B}$: QGP phase pressure P must be *negative* when the dynamical pressure comprising effect of the flow runs its course, $\mathcal{P} \rightarrow 0$. A fireball surface region which reaches $\mathcal{P} \rightarrow 0$ but for which $v \neq 0$, i.e., it continues to flow outward, is torn apart in a rapid filamentation instability. This situation can *only* arise since the quark-gluon matter presses again the collective vacuum which is not subject to collective dynamics.

Phase boundary between the hadron gas domain and quark-gluon plasma, which includes the effect of the ‘wind’ of flow of QCD matter is shown in figure 24, for a geometric model with $\kappa = 0.6$. With increasing flow velocity the phase boundary set at $\mathcal{P} \rightarrow 0$ moves to lower temperatures. This effect is larger near to $\mu_b = 0$ than the effect μ_b has on change in T . We can now understand the behavior seen in figure 23: at RHIC there is the largest supercooling and the flow velocity is greatest, yielding smallest hadronization temperature. As collective flow velocity decreases, the hadronization temperature increases, though this effect is somewhat compensated by the influence of the the increase in μ_b which implies a decrease in T . The impact of the flow velocity is smallest near to 80A collision energy, where the hadronization temperature is nearly reaching the HG–QGP phase boundary.

This would not suggesting that the onset of QGP formation is in the collision energy window 40–80A GeV. This would be in conflict with the result shown in last line of table 4, where we present the experimental result for

$$K/\pi \equiv \sqrt{K^+/\pi^+ \times K^-/\pi^-}. \quad (25)$$

The advantage of taking the geometric mean of the charged kaon to pion ratios is that the chemical potentials of strangeness and baryon number cancel in Boltzmann

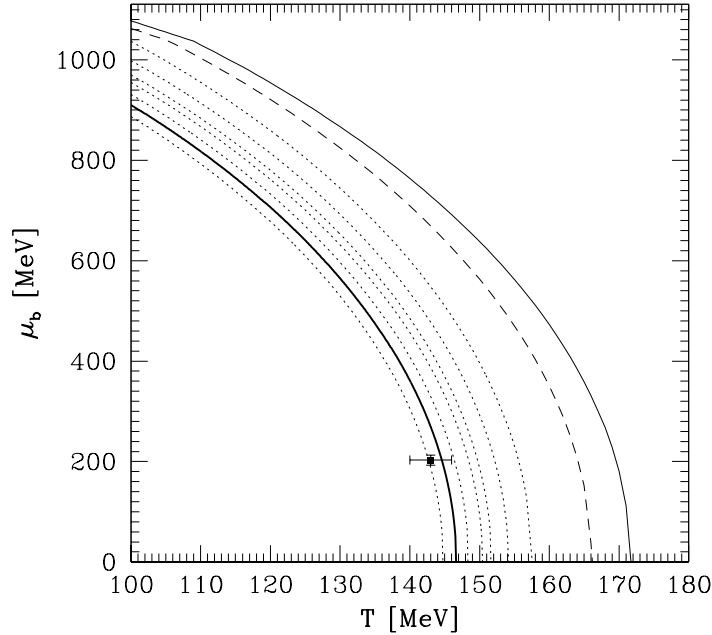


Figure 24. Hadronization boundary in the μ_b, T plane: solid (point hadrons) and dashed (finite volume hadrons) lines are estimates of QGP–HG boundary for a system at rest. Dotted lines are for finite size hadrons and include collective flow velocity for $v^2 = 0, 1/10, 1/6, 1/5, 1/4, 1/3$. Thick solid line: breakup with $v = 0.54, \kappa = 0.6$ [41]. The measured point relates to the hadronization condition at $158A$ GeV.

approximation. The constant value we see at SPS leaves no space for any discontinuity in strangeness production in SPS energy range, including the newly available result at 30 GeV [12]. This finding contradicts the claim that the rise of K^+/π^+ ratio with decreasing collision energy suggests new physics occurring near $30A$ GeV [57] (but does not contradict the fact, which is claimed on false grounds). The consideration of K/π indicates that the variation of the baryochemical and strangeness chemical potentials fully account for peak in K^+/π^+ production.

The increase in K/π ratio between RHIC and SPS energies is an indicator of new physics, and an energy scan between RHIC and SPS energies would at first seem appropriate. However, the 40% increase we see moving on from SPS to RHIC has been in this paper understood as the result of the initial state changes and faster, more explosive expansion of the fireball. Still, it would be good to make sure that this rise is not step-like, which would suggest a phase change.

Our findings make the issue where is the onset of QGP formation at first enigmatic. We have seen that specific per baryon strangeness and entropy are both evolving smoothly in the energy range beginning at $40A$ GeV and through the RHIC energies. We see in figure 23 that near $80A$ GeV supercooling seizes, and below this collision energy the particle freeze-out occurs in HG phase. This means that if QGP phase is formed below $80A$ GeV, there is reequilibration of particle yields. Still, we expect that strangeness yield would be preserved, and any enhancement of strangeness

to entropy yield as expressed by the K/π ratio equation (25) should remain visible.

The top AGS energy at $11.6A$ GeV for the Au beam yields [58]:

$$K/\pi = 0.077.$$

An increase of AGS result by 55% is required to reach the SPS level present at $30A$ GeV. This increase is sufficiently sudden to suggest that a change in reaction mechanism must occur between 30 and $10A$ GeV beam energy. Since the only change we are expecting is the onset of deconfinement, we have all reason to hope that a rather sudden rise in K/π can be observed in this energy domain. Naturally we also expect that evolution of specific strangeness and entropy production will show a sudden increase in this energy domain.

7. Anything new at LHC?

An often posed question is if there can be a future for strangeness as signature of QGP at the LHC energy scale which is 30 times greater than at RHIC. In principle, one would think that the extreme conditions expected will reduce the importance of strangeness as diagnostic tool, since the difference between u, d and s flavors will diminish. We do not believe that charm and bottom flavors will ‘replace’ strangeness as an observable, rather these new degrees of freedom produced in first collisions will complement the physics potential of strangeness, which as we now argue, will further grow at LHC.

The QGP based production processes at RHIC lead to a highly oversaturated strangeness phase space yield. The mechanisms responsible for this are likely to augment as the energy available in the nuclear collision increases: it is probable that at LHC we reach greater initial temperatures and more explosive transverse flow. As the system volume expands, but entropy remains nearly conserved, there is significant reduction of particle pairs. Since the reannihilation of light quarks is favored by cross section, compared to the reannihilation of more massive strange quarks, this faster expansion is driven predominantly by the energy derived from light flavors. Strange quarks, once produced should remain more if not mostly preserved till the hadronization.

As a consequence, we expect that γ_s/γ_q will further increase at LHC compared to the large RHIC value, which at $\sqrt{s} = 130A$ GeV is about 1.5. An increase in this ratio triggers an increase in the yield of kaons, as compared to pions. At the nearly baryon free conditions prevailing at LHC, we can consider $\lambda_q = \lambda_s = 1$, hence the value of K^\pm/π^\pm ratio in a statistical hadronization model is proportional solely to γ_s/γ_q and depends on the hadronization temperature T . When $\gamma_s = \gamma_q = 1$, this ratio as function of T is shown in figure 25 as dashed line. This chemical equilibrium result applies also at finite baryon density (SPS) to the geometric mean of the charged particle ratios, equation (25). At $T \simeq 160$ MeV, we see in figure 25 $K/\pi \simeq 0.133$.

The solid line, in figure 25, shows the maximum possible value of K/π ratio, with both γ_s and γ_q increasing to the maximum allowed by the requirement that neither kaon nor pions condensation arises, compare equation (19):

$$\gamma_s \gamma_q = e^{m_K/T}, \quad \gamma_q \gamma_q = e^{m_\pi/T}, \text{ for } \lambda_q = \lambda_s = 1.$$

The arrow indicates where the lines will meet at very large hadronization temperatures. The exact location of this limit is in part result of yet limited knowledge of hadronic high mass resonances. In fact, it can be suspected that the slight decrease in the

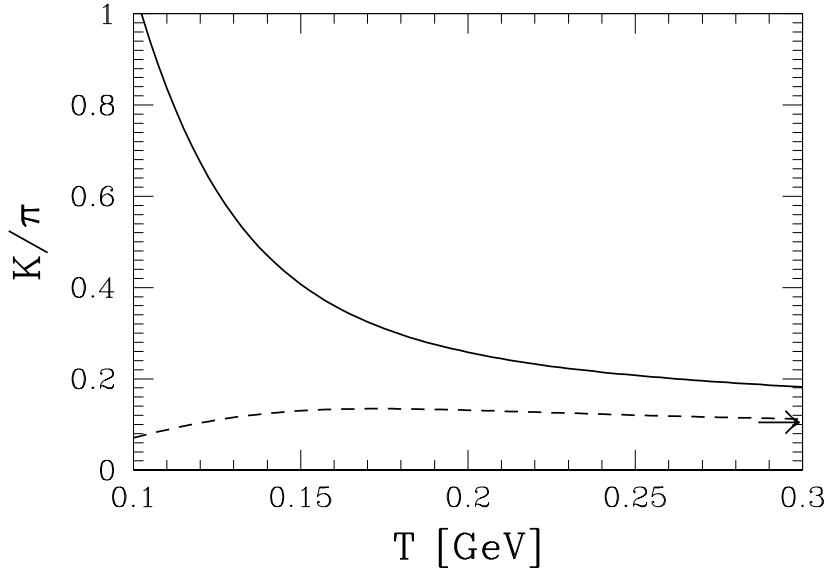


Figure 25. Kaon to pion ratio (see text) as function of hadronization temperature for chemical equilibrium (dashed line) and with maximum allowable γ_s and γ_q (solid line).

ratio K/π with increasing hadronization temperature is spurious, originating from our lack of knowledge of the hadron strange and non-strange mass spectra. Moreover, it can be expected that hadronization temperature remains at or below the Hagedorn temperature $T \simeq 160$ MeV at LHC.

The important result we see is that K/π can almost triple without violating any fundamental principles, in a scenario in which initial thermal and very hot QGP phase is formed and expands explosively. Of course, this does not prove that this will happen at LHC, though a significant increase of K/π should occur. Perhaps more spectacular is the expected rise in the Wróblewski ratio W_s , which compares the effectiveness of strange quark production to light quark production [51], counting only newly made quark pairs, compare equation (20) and figure 17. $W_s \simeq 0.2\text{--}0.25$ in $p\text{-}p$ reactions expressing the low yield of strange quark pairs available. In heavy ion collisions, values as large as triple this result have been observed, expressing, as discussed, the large enhancement of strangeness yield as compared to light quark yield. Somewhat smaller W_s values are expected in chemical equilibrium in baryon-free matter, as shown by dashed line in figure 26. The solid line, in figure 26, shows the great enhancement of W_s should maximal overpopulation of strange quark phase space indeed be established (note logarithmic scale in figure 26). The arrow indicates the large T limit of W_s which against naive expectation is found somewhat below unity. This is an expression of the asymmetry in the number of undiscovered strange and non-strange high mass hadron resonances. Again, this is a purely academic point, as hadronization is expected at or below the Hagedorn temperature $T \simeq 160$ MeV.

The new physics presented in this report, include a consistent chemical non-equilibrium analysis of the SPS and RHIC experimental results which shows great consistency of physical properties and reaction mechanism in these two domains. We have demonstrated that the great enhancement of strangeness production at RHIC

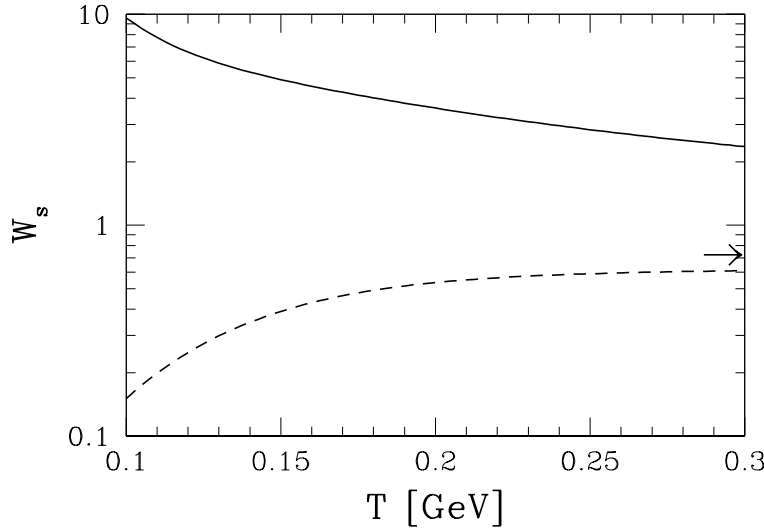


Figure 26. Wróblewski ratio W_s for chemical equilibrium (dashed line) and maximum allowable γ_s and γ_q in baryon-free matter.

is originating in the same mechanism as strangeness production at SPS. We have illustrated how low hadronization temperatures derive from supercooling due to the fast collective flow of deconfined matter, and we have above presented a possible scenario for a large strangeness anomaly at LHC.

Acknowledgments

Supported by a grant from the U.S. Department of Energy, DE-FG03-95ER40937. Laboratoire de Physique Théorique et Hautes Energies, LPTHE, at University Paris 6 and 7 is supported by CNRS as Unité Mixte de Recherche, UMR7589.

References

- [1] Letessier J and Rafelski J 1999 *Phys. Rev. C* **59** 947
- [2] Letessier J and Rafelski J 2000 *Int. J. Mod. Phys. E* **9** 107
- [3] Letessier J and Rafelski J *Hadrons and Quark-Gluon Plasma* Cambridge Monogr. Part. Phys. Nucl. Phys. Cosmol., **18** 2002.
- [4] Rafelski J and Letessier J 2002 *Nucl. Phys. A* **702** 304
- [5] Rafelski J and Letessier J 2002 *Nucl. Phys. A* **715** 98c
- [6] Appelshäuser H *et al* (NA49 collaboration) 1998 *Phys. Lett. B* **444** 523
- [7] Afanasev S V *et al* 2001 *J. Phys. G* **27** 367
- [8] Afanasev S V *et al* Energy dependence of Λ and $\bar{\Lambda}$ production at CERN-SPS energies 2002 *Preprint* nucl-ex/0209002
- [9] Afanasev S V *et al* 2002 *Phys. Lett. B* **538** 275
- [10] Alessandro B *et al* 2003 *Phys. Lett. B* **555** 147
- [11] Hohne C *et al* System size dependence of strangeness production at 158-AGeV 2002 *Preprint* nucl-ex/0209018
- [12] Gazdzicki M 2003 Compilation of NA49 results as function of collision energy Private communication
- [13] Andersen E *et al* (WA97 collaboration) 1999 158A GeV. *Phys. Lett. B* **449** 401
- [14] Antinori F *et al* (WA85 collaboration) 1999 *Phys. Lett. B* **447** 178
- [15] Antinori F *et al* (WA97 collaboration) 2000 *Nucl. Phys. A* **663** 717

- [16] Antinori F *et al* 2002 Results on Λ and Ξ production in Pb Pb collisions at 160-GeV/c per nucleon from the NA57 experiment *Preprint hep-ex/0207047*
- [17] Rafelski J and Müller B 1982 *Phys. Rev. Lett.* **48** 1066 See also *Phys. Rev. Lett.* **56** 2334E 1986
- [18] Koch P Müller B and Rafelski J 1986 *Z. Phys. A* **324** 453
- [19] Letessier J Rafelski J and Tounsi A 1996 *Phys. Lett. B* **389** 586
- [20] Rafelski J and Letessier J 1999 *Phys. Lett. B* **469** 12
- [21] Biró T and Zimányi J 1982 *Phys. Lett. B* **113** 6
- [22] Biró T Lukács B and Zimányi J 1982 *Nucl. Phys. A* **386** 617
- [23] Adler C *et al* 2002 *Phys. Rev. Lett.* **89** 132301
- [24] Rafelski J 1982 *Phys. Rep.* **88** 331
- [25] Rafelski J and Danos M 1987 *Phys. Lett. B* **192** 432
- [26] Rafelski J 1984 *Nucl. Phys. A* **418** 215c
- [27] Åkesson T *et al* (AFS-ISR collaboration) 1984 *Nucl. Phys. B* **246** 1
- [28] Alner *et al* (UA5 collaboration) 1985 *Phys. Lett. B* **151** 309
- [29] Alexopoulos T *et al* (E-735 collaboration) 1990 *Phys. Rev. Lett.* **64** 991
- [30] Huang H Z 2002 *Nucl. Phys. A* **698** 663
- [31] Castillo J 2002 *J. Phys. G* **28** 1987
- [32] Alber T *et al* (NA35 collaboration) 1994 *Z. Phys. C* **64** 195
- [33] Alber T *et al* (NA35 collaboration) 1996 *Phys. Lett. B* **366** 56
- [34] Di Bari D *et al* (WA85 collaboration) 1995 *Nucl. Phys. A* **590** 307c
- [35] Antinori F *et al* (WA97 collaboration) 2000 *Eur. Phys. J. C* **14** 633
- [36] Bearden I G *et al* (NA44 collaboration) 1997 *Phys. Rev. Lett.* **78** 2080
- [37] Torrieri G and Rafelski J 2001 *New J. Phys.* **3** 12
- [38] Rafelski J 1991 *Phys. Lett. B* **262** 333
- [39] Csörgő T and Csernai L P 1994 *Phys. Lett. B* **333** 494
- [40] Csernai L P and I N Mishustin I N 1995 *Phys. Rev. Lett.* **74** 5005
- [41] Rafelski J and Letessier J 2000 *Phys. Rev. Lett.* **85** 4695
- [42] Thews R L 2003 Private communication
- [43] Torrieri G and Rafelski J 2003 A comparison of statistical hadronization models *J. Phys. G* in press
- [44] Fermi E 1953 *Phys. Rev.* **92** 452
- [45] Adler C *et al* 2002 *Phys. Rev. Lett.* **89** 092301
- [46] Fachini P 2002 *J. Phys. G* **28** 1599
- [47] Zhang H 2003 $K^{*0}(892)$ resonance production in Au+Au and collisions at $\sqrt{s_{NN}} = 200$ -GeV *J. Phys. G* in press
- [48] Markert C 2002 *J. Phys. G* **28** 1753
- [49] Rafelski J Letessier J and Torrieri G 2001 *Phys. Rev. C* **64** 054907
- [50] Koch P Rafelski J and Greiner W 1983 *Phys. Lett. B* **123** 151
- [51] Wróblewski A K 1985 *Acta Phys. Pol. B* **16** 379
- [52] Becattini F Cleymans J Keranen A Suhonen E and Redlich K 2001 *Phys. Rev. C* **64** 024901
- [53] Letessier J and Rafelski J 2003 *Phys. Rev. C* **67** 031902
- [54] Fodor Z and Katz S D 2002 *Phys. Lett. B* **534** 87
- [55] Fodor Z and Katz S D 2002 *J. High Energy Phys.* **203** 14
- [56] Fodor Z Katz S D and Szabo K K 2002 The QCD equation of state at nonzero densities: Lattice result *Preprint hep-lat/0106002*
- [57] Gazdzicki M 2003 Energy scan program at CERN SPS *J. Phys. G* in press
- [58] L. Ahle *et al* (E802 collaboration) 1999 *Phys. Rev. C* **58** 3523